JAERI-M
88-043

EXPERIMENTAL TRANSPORT ANALYSIS CODE SYSTEM IN JT-60

March 1988

Toshio HIRAYAMA, Katsuhiro SHIMIZU, Keiji TANI
Hiroshi SHIRAI and Mitsuru KIKUCHI

日 本 原 子 力 研 究 所
Japan Atomic Energy Research Institute

JAERI-Mレポートは，日本原子力研究所が不定期に公刊している研究報告書です。
入手の問合わせは，日本原子力研究所技術情報部情報資料課（〒319－11茨城県那珂郡東海村）あて，お申しこしください。なお，このほかに財団法人原子力弘済会資料センター（〒319-11茨城県那珂郡東海村日本原子力研究所内）で複写による実費頒布をおこなっております。

JAERI-M reports are issued irregularly.
Inquiries about availability of the reports should be addressed to Information Division, Department of Technical Information, Japan Atomic Energy Research Institute, Tokai-mura, Naka-gun, Ibaraki-ken 319-11, Japan.

編集兼発行　日本原子力研究所
印　　刷　日立高速印刷株式会社

JAERI-M 88-043

Experimental Transport Analysis Code System in JT-60

Toshio HIRAYAMA, Katsuhiro SHIMIZU, Keiji TANI
Hiroshi SHIRAI and Mitsuru KIKUCHI

Department of Large Tokamak Research
Naka Fusion Research Establishment
Japan Atomic Energy Research Institute
Naka-machi, Naka-gun, Ibaraki-ken

(Received February 1, 1988)

Transport analysis codes have been developed in order to study confinement properties related to particle and energy balance in ohmically and neutral beam heated plasmas of JT-60. The analysis procedure is divided into three steps as follows:

1) LOOK ; The shape of the plasma boundary is identified with a fast boundary identification code of FBI by using magnetic data, and flux surfaces are calculated with a MHD equilibrium code of SELENE. The diagnostic data are mapped to flux surfaces for neutral beam heating calculation and/or for radial transport analysis.
2) OFMC ; On the basis of transformed data, an orbit following Monte Carlo code of OFMC calculates both profiles of power deposition and particle source of neutral beam injected into a plasma.
3) SCOOP ; In the last stage, a one dimensional transport code of SCOOP solves particle and energy balance for electron and ion, in order to evaluate transport coefficients as well as global parameters such as energy confinement time and the stored energy.

The analysis results are provided to a data bank of DARTS that is used to find an overview of important consideration on confinement with a regression analysis code of RAC.

Keywords : Tokamak, JT-60, Transport analysis, LOCK, OFMC, SCOOP, LIBRARY, DARTS, RAC

ＪＴ−60実験における輸送解析コードシステム

日本原子力研究所那珂研究所臨界プラズマ研究部
平山　俊雄・清水　勝宏・谷　　啓二
白井　　浩・菊池　　満

（1988年2月1日受理）

オーミック加熱，および中性粒子入射により加熱されたＪＴ−60のプラズマについて，粒子及びエネルギー・バランスにかかわる閉じ込め特性を解析するために，輸送解析コードが開発された。解析の手順は以下に示すように，いくつかの段階に分かれている：

1）　ＬＯＯＫ　；　プラズマ境界の形状はＦＢＩというコードにより求められる。磁気面は，ＭＨＤ平衡コードＳＥＬＥＮＥにより計算される。計測データはこの磁気面上に変換され，中性粒子ビーム加熱計算，あるいは，径方向の輸送解析用のデータとなる。

2）　ＯＦＭＣ　；　変換されたデータを用いて，モンテカルロ軌道追跡コードによりプラズマ中に入射された中性粒子ビームの加熱パワー分布，及び粒子源の分布を計算する。

3）　ＳＣＯＯＰ　；　最後に，一次元輸送コードＳＣＯＯＰにより，電子とイオンのエネルギーバランスを解いて輸送係数を求める。また，エネルギー閉じ込め時間及び蓄積エネルギーといったグローバル量が計算される。

解析結果はデータ・バンク・ＤＡＲＴＳに登録され，回帰分析コードＲＡＣにより閉じ込め特性の相関などを調べることができる。

那珂研究所：〒311-01 茨城県那珂郡那珂町大字向山801-1

Contents

目　　次

1. Introduction

Now, in a study of tokamak plasmas, many kinds of calculation codes have been developed and have produced a powerful way to understand the tokamak plasma. These codes are very useful not only for theoretical research but also for experimental one, since these codes will enable us to extract as much physical meanings as possible from limited experimental data and to seek the direction of future experiments.

Basic idea of the empirical analysis of the transport properties of tokamaks are described in a few papers[1,2]. The transport properties of tokamak plasmas should depend on the transport coefficients. However, theoretical efforts to find the transport coefficients in tokamaks have not yet provided a reliable formula predicting the confinement properties of tokamaks. Transport coefficients derived by using the experimental data seems to be more reliable than those derived from the theoretical research.

Confinement analysis procedures in JT-60 are divided into a few steps illustrated in Fig.1. The shape of the plasma boundary is identified at first with the FBI(Fast Boundary Identification) code, in which macroscopic equilibrium quantities such as major radius R_p, minor radius a_p, Shafranov Λ $(=\beta_p+l_i/2)$ and surface voltage V_s are evaluated by using magnetic data. The equilibrium flux surface is calculated by SELENE[3] (numerical equilibrium code) using the identified plasma boundary. The SELENE seeks a numerical solution of the Grad-Shafranov equation in the rectangular grids, without employing the moment method. A position of the diagnostic data is recognized at the flux coordinates and radial profiles of electron temperature T_e, electron density n_e and radiation loss P_r are obtained by the least square fitting technique. On the basis of T_e, n_e and τ_p (particle confinement time), the power deposition and particle source profiles are evaluated on the flux surfaces with the OFMC(Orbit Following Monte-Carlo) code that can precisely calculate a loss fraction of NB power due to charge exchange reactions as well as loss orbits. Above quantities calculated by both codes are mapped to data in the one-dimensional coordinate in order to solve the radial energy balances for the electron and the ion. A one-dimensional transport code of SCOOP analyzes the data and calculates global parameters such as energy confinement time τ_E and stored energy W_s, in addition to the transport coefficients. Major parameters of the analyzed data are stored into the confinement data bank and are used for

finding the correlation between various shots.

The description of the diagnostic interface code LOOK is given in section 2 and that of the neutral beam code OFMC is shown in section 3. The descriptions of the one-dimensional radial transport code SCOOP and the data bank system are shown in sections 4 and 5.

2. LOOK : Diagnostic Interface Code

2.1 Diagnosis for Confinement Analysis

Various diagnostic data are useful for the empirical analysis of transport properties of tokamak plasmas.

Radial profile of the electron temperature Te(r) is measured by the multipulse Thomson scattering system and ECE foulier spectrometers. Radial profile of the electron density $n_e(r)$ is measured by the Thomson scattering and 4 channel interferometers. Ion temperature is measured by the doppler broadening of the heavy impurity(crystal spectrometer), charge exchange energy spectrum and the doppler broadening of the He active beam probe. Particle confinement time τ_p is measured by the 3 channel H_α photo-diodes. Radiation is measured by 15 channel bolometer array.

Typical equilibrium configuration and the rough sketch of the diagnostics available for the confinement analysis are shown in Fig.2.

2.2 Magnetic Analysis of Plasma Equilibrium

Magnetic analysis of the plasma equilibrium gives a basic transformation relation of the Diagnostics data between cylindrical coordinates and flux coordinates. The shape of the plasma boundary in divertor and limiter equilibrium is analyzed by the FBI (Fast Boundary Identification) code in which measured values of I_p(plasma current), I_c(poloidal coil currents, c=F,V,H,Q,M), I_T(toroidal coil current) and B_{pj}, $B_{\omega j}$(poloidal magnetic field outside the plasma, j=1,6) are used to find the outermost flux surface and the equilibrium field quantities such as q_{eff} and Λ. The flux surface geometry inside the plasma is obtained from the fixed boundary numerical solution or a simplified moment solution to the Grad-Shafranov equation. Current density profile in the numerical analysis is assumed as

finding the correlation between various shots.

The description of the diagnostic interface code LOOK is given in section 2 and that of the neutral beam code OFMC is shown in section 3. The descriptions of the one-dimensional radial transport code SCOOP and the data bank system are shown in sections 4 and 5.

2. LOOK : Diagnostic Interface Code

2.1 Diagnosis for Confinement Analysis

Various diagnostic data are useful for the empirical analysis of transport properties of tokamak plasmas.

Radial profile of the electron temperature Te(r) is measured by the multipulse Thomson scattering system and ECE foulier spectrometers. Radial profile of the electron density $n_e(r)$ is measured by the Thomson scattering and 4 channel interferometers. Ion temperature is measured by the doppler broadening of the heavy impurity(crystal spectrometer), charge exchange energy spectrum and the doppler broadening of the He active beam probe. Particle confinement time τ_p is measured by the 3 channel H_α photo-diodes. Radiation is measured by 15 channel bolometer array.

Typical equilibrium configuration and the rough sketch of the diagnostics available for the confinement analysis are shown in Fig.2.

2.2 Magnetic Analysis of Plasma Equilibrium

Magnetic analysis of the plasma equilibrium gives a basic transformation relation of the Diagnostics data between cylindrical coordinates and flux coordinates. The shape of the plasma boundary in divertor and limiter equilibrium is analyzed by the FBI (Fast Boundary Identification) code in which measured values of I_p(plasma current), I_c(poloidal coil currents, c=F,V,H,Q,M), I_T(toroidal coil current) and B_{pj}, $B_{\omega j}$(poloidal magnetic field outside the plasma, j=1,6) are used to find the outermost flux surface and the equilibrium field quantities such as q_{eff} and Λ. The flux surface geometry inside the plasma is obtained from the fixed boundary numerical solution or a simplified moment solution to the Grad-Shafranov equation. Current density profile in the numerical analysis is assumed as

$J_\varphi \propto -(\beta_p R+(1-\beta_p)R_p^2/R)\ (1-(\psi-\psi_{ax})/(\psi_s-\psi_{ax}))^n$ where ψ_{ax} and ψ_s are poloidal fluxes at magnetic axis and plasma surface, respectively. Unknown parameter n is matched to the assumed l_i value and β_p is assumed as $\beta_p = \Lambda_{FBI}-l_i$. Faraday rotation angle is also calculated for the comparison with the measurement. For the simplified moment solution, flux surface including radial shift ($\Delta(\rho)$) and ellipticity ($E(\rho)$) are used and the outermost flux surface is matched with FBI code.

2.3 Flux Surface Transformation and Least Square Fit

The diagnostic data such as T_e , n_e , P_r are assumed to be constant on a flux surface. Using the flux surface obtained in section 3-2, it is easy to identify the flux surface of the Thomson scattering and ECE data points. On the other hand, FIR interferometers and the bolometer array gives line-integrated physical quantities. We use the least square fitting technique to get the radial profile of the electron density and the radiation profile. The radial coordinate r used in the 1-D radial transport analysis is defined as $r = \sqrt{V(\psi)/(2\pi^2 R_p)}$
where $R_p = V(\psi_s)/(2\pi S(\psi_s))$, $S(\psi)$ and $V(\psi)$ are the poloidal cross section and the volume inside the flux surface.

Electron density profile is assumed to be $n_e(r) = n_{e0}(1-(r/a_p)^2)^m$ where n_{e0} and m are the unknown parameters and are determined so that $L(n_{e0},m) = \Sigma(\int n_e dl_i^{cal}-\int n_e dl_i^{meas})^2$ is minimized with respect to n_{e0} and m .

Bolometer signal $S_{bol\,i}$ gives the line integral of the radiation inside the plasma $S_{bol\,i} = \int P_r dl_i$ where P_r is the local radiation power density. A linear matrix relation between P_r and S_{bol} can be obtained by $S_{bol\,i} = \Sigma D_{ij}P_{rj}$. Unknown parameters P_{rj} are determined so that $L(P_{rj}) = \Sigma(S_{bol\,i}^{cal}-S_{bol\,i}^{meas})^2$ is minimized with respect to P_{rj}. This minimization gives a following matrix equation for P_{rj}

$$H\ P_r = F$$

where, $H_{jk} = \Sigma D_{ij}D_{ik}$ and $F_j = \Sigma D_{ij}S_{bol\,i}^{meas}$. The electron temperature profile $T_e(r)$ is fitted with the polynomial $T_e = T_{e0}\ (1-(r/a_p)^2+\alpha(r/a_p)^2(1-r/a_p)+\beta(r/a_p)^2(1-(r/a_p)^2))$ and unknown parameters T_{e0}, α and β are determined so that $L(T_{e0},\alpha,\beta) = \Sigma(T_{ei}^{meas}-T_{ei}^{cal})^2$ is minimized with respect to T_{e0}, α and β. This minimization is analytically obtained as follows,

$$\alpha = (H_{22}g_1 - H_{12}g_2)/D$$

$$\beta = (H_{11}g_2 - H_{21}g_1)/D$$

$$T_{e0} = \Sigma T_{ei}^{meas} \cdot (\alpha F_1 + \beta F_2 + F_3) / \Sigma(\alpha F_1 + \beta F_2 + F_3)^2$$

where,

$$H_{lk} = \Sigma A_{jk} A_{jl} \quad (l,k=1,2)$$

$$g_k = -\Sigma A_{jk} A_{j3} \quad (k=1,2)$$

$$D = H_{22}H_{11} - H_{12}H_{21}$$

$$A_{jk} = T_{ej}^{meas} \cdot S_k - F_k$$

$$S_k = \Sigma T_{ei}^{meas} \cdot F_k / \Sigma T_{ei}^{meas\,2}$$

$$F_1 = (r/a_p)^2(1-r/a_p), F_2 = (r/a_p)^2(1-(r/a_p)^2), \quad F_3 = 1-(r/a_p)^2$$

Typical density and temperature profiles for both limiter and divertor discharges are shown in Fig.3. The density profiles obtained by the 4 channel interferometers are consistent with the Thomson scattering measurement.

2.4 Output Specification

The LOOk code provides the contour plot of the flux surface , the magnetic summary (R_p, a_p , I_p , B_t , δ_{30} , Λ etc.) , electron stored energy , ohmic input power and radial profiles of T_e , n_e , P_r of a particular time of interest and I_p-V_L-$\int n_e dl$ wave forms. Typical example of the output is shown in Fig.4.

The magnetic data and T_e-n_e-P_r transformed into the 1-D radial coordinate are stored in a binary data file (SCOOP data) which is called by the SCOOP code described in section 4. Look code provides plasma parameter file and the flux surface table for the neutral beam injection heating analysis(OFMC code).

3. OFMC : Orbit Following Monte Carlo Code

3.1 Neutral Beam Injection Heating

The thermalization process of fast ions is described by the drift kinetic equations with Fokker-Planck collision terms of Landau form. In an axisymmetric system, the projection chart of the collisionless guiding center orbit on a poloidal cross section shows a completely closed contour. This enables us to solve analytically the above mentioned equations after linearizing and averaging them over the bounce time of fast ions. Many authors have adopted this method to solve the slowing-down process of fast ions produced by NBI[4)-7)] or charged fusion products[8)]. In the presence of ripple, however, the guiding center orbit never closes and consequently the loss process of fast ions is seriously affected by the unclose collisionless orbits. This makes it very difficult to apply the theoretical method to solve the relaxation process of fast ions in a non-axisymmetric system. To make a precise treatment of this kind of problem, an orbit-following Monte-Carlo simulation code has been newly developed, in which the calculation of Coulomb collisions is executed at every several time steps of orbit calculation (1/10~1/50 bounce time) until the test particle slows down to the local ion temperature of bulk plasma.

For the convenience of calculations, following assumptions are made. The background plasma parameters are immutable during the slowing-down time τ_s. Both distribution functions of bulk plasma ions and electrons are Maxwellian. There is no electric field in the plasma.

Objectives of the present works are; 1) to investigate the thermalization process of fast ions with large banana size, 2) to estimate the charge exchange loss of fast ions during slowing down, 3) to study the effect of loss orbits in an axisymmetric magnetic field as well as in a non-axisymmetric field on the power loss of NBI, 4) to investigate the NBI relevant phenomena such as plasma current induction, plasma rotation, and 5) to interpret the diagnostic results of CX loss neutrals and neutrons.

3.2 Calculation model

(1) Birth distribution of fast ions Fast neutral atoms injected into an

ohmically heated plasma are ionized or charge exchanged by interactions with field plasma ions and electrons. The fraction of neutral beams which is trapped in a plasma can be described by[9]

$$S = \sum_k \gamma_k \int_0^{L_{max}} \int_0^{2\pi} \int_0^{a_b} f(r_b,\theta_b) \exp\left[-\int_0^{L_b} n_e(r)\sigma_i(E_b/k)dL\right] \times n_e(r)\sigma_i(E_b/k) r_b dr_b d\theta_b dL_b, \quad (3\text{-}1)$$

where r_b,θ_b are polar co-ordinates in the beam cross section perpendicular to the beam line, L_b the beam path length, L_{max} the maximum beam path length which intersects the plasma column, a_b the neutral beam radius, E_b the primary beam energy, γ_k the density fraction of beam atoms with energy of E_b/k, σ_i the total ionization cross section, and $f(r_b,\theta_b)$ the normalized distribution of beam density which gives

$$\int_0^{a_b} \int_0^{2\pi} f(r_b,\theta_b) r_b dr_b d\theta_b = 1.0 \ .$$

Provided that the cross section for ionization of atomic hydrogen by stripped impurity ions is of the form[10,11]

$$\sigma_z = Z_{imp}^{1.4}(\sigma_p + \sigma_{cx}),$$

where σ_p is the ionization cross section of atomic hydrogen by protons, σ_{cx} the cross section for charge exchange by protons in atomic hydrogen[12] and Z_{imp} the charge number of impurity ions. Then the total ionization cross section is given by

$$\sigma_i = \sigma_e + (\sigma_p + \sigma_{cx})[f_i + (1 - f_i)^{0.6} (Z_{eff} - f_i)^{0.4}],$$

where σ_e is the cross section for ionization of atomic hydrogen by electrons, Z_{eff} the effective Z and $f_i = n_i/n_e$.

Here we consider a circular cross-sectional neutral beam with

$$f(r_b,\theta_b) = \frac{C_g}{\pi a_b^2} \exp[1 - (r_b/a_b)^2], \quad (3\text{-}2)$$

where $c_g = e/(e-1)$. Introducing new variables

$$r_b' = \sqrt{c_g[1-exp(-(r_b/a_b)^2)]}$$

$$\theta_b' = \theta_b/2\pi$$

$$L_b' = L_b/L_{max}$$

and substituting eq.(3-2) into eq.(3-1), we obtain

$$S = 2L_{max}\sum_k \gamma_k \int_0^1\int_0^1\int_0^1 \exp\left[- L_{max}\int_0^{L_b} n_e(r)\sigma_i(E_b/k)dL\right] \times n_e(r)\sigma_i(E_b/k)r_b'dr_b'd\theta_b'dL_b'. \quad (3\text{-}3)$$

Since the total number of test particles is limited within about 2000 due to the long computational time, the Monte-Carlo integration method is again adopted to calculate S numerically, in which five uniform random numbers corresponding to r_b, θ_b, L_b, beam ion species k, and co-injection fraction are generated for every sampling point (≡ test particle).

(2) Guiding center orbit

Ion trajectories are followed by numerical integration of the standard guiding center equations of motion[13] The guiding center equations are

$$\vec{v}_g = \frac{1}{Z_t e}\left(\mu_m + \frac{m_t}{B} v_{g\parallel}^2\right)\frac{\vec{B}}{B}\times\frac{\nabla B}{B} + \frac{\vec{B}}{B} v_{g\parallel}, \quad (3\text{-}4)$$

$$\frac{dv_{g\parallel}}{dt} = - \frac{\mu_m}{m_t}\frac{\partial B}{\partial l}, \quad (3\text{-}5)$$

where $v_{g\parallel}$ and $v_{g\perp}$ are the guiding center velocities parallel and perpendicular to the magnetic field line, l the length along the field line, m_t the charged particle mass, Z_t the charge number , $e = 1.6\times10^{-19}C$, μ_m the magnetic moment, and B the total magnetic field, respectively. The method of Runge-Kutta (second order) is adopted to the numerical integration.

The axisymmetric components of magnetic field are given by the derivatives of ψ which is obtained by the diagnostic interface code of LOOK. To obtain the distribution of the field ripple, we consider a model toroidal

coil current which is a sheet current on a torus with ripple component. The field ripple is calculated by the method of Biot-Savart.

(3) Calculation of Coulomb collisions

The collisional process of fast ions has been simulated by a technique of Monte-Carlo. Provided that a test particle change its velocity components parallel and perpendicular to the magnetic field line from ($v_{\parallel}$, $v_{\perp}$) to ($v_{\parallel}'$, $v_{\perp}'$) by collision with field particles as shown in Fig. 5, relations among these velocity components are given by

$$v_{\parallel}' = v_{\parallel} + \Delta v_l \frac{v_{\parallel}}{v} - \Delta v_t \frac{v_{\perp}}{v} \sin\Omega \ , \tag{3-6}$$

$$v_{\perp}' = [(v + \Delta v_l)^2 + \Delta v_t^2 - v_{\parallel}'^2]^{1/2} \ , \tag{3-7}$$

where v ($= \sqrt{v_{\parallel}^2 + v_{\perp}^2}$) is the total velocity of the test particle, Ω the Larmor phase, Δv_l the longitudinal component of the velocity change, and Δv_t the transverse component, respectively. The velocity changes Δv_l and Δv_t result from the slowing-down and pitch-angle scattering of the test particles due to Coulomb collision with field particles. Under the assumption that the field particles have a Maxwellian velocity distribution, the mean values and mean square deviations of Δv_l and Δv_t are given by[14]

$$\frac{<\Delta v_l>}{v_\beta} = -\frac{3}{2}\sqrt{\pi}\, M_t \frac{\Delta t}{\tau_s} \sum_p Z_p^2 \frac{m_p+m_t}{m_t} \frac{n_p'}{T_p'} \frac{\mu(\chi_p)}{2\chi_p} \ , \tag{3-8}$$

$$\frac{<\Delta v_t>}{v_\beta} = 0.0 \tag{3-9}$$

$$\frac{<\Delta v_l^2>}{v_\beta^2} = \frac{3}{2}\sqrt{\pi}\, M_t \frac{\Delta t}{\tau_s} \sum_p Z_p^2 \frac{m_p^{1/2}}{m_t^{1/2}} \frac{n_p'}{T_p'^{1/2}} \frac{\mu(\chi_p)}{2\chi_p^{3/2}} \ , \tag{3-10}$$

$$\frac{<\Delta v_t^2>}{v_\beta^2} = \frac{3}{2}\sqrt{\pi}\, M_t \frac{\Delta t}{\tau_s} \sum_p Z_p^2 \frac{m_p^{1/2}}{m_t^{1/2}} \frac{n_p'}{T_p'^{1/2}} \left[\mu(\chi_p) + \frac{d\mu(\chi_p)}{d\chi_p} - \frac{\mu(\chi_p)}{2\chi_p} \right] \frac{1}{\chi_p^{1/2}} \ , \tag{3-11}$$

where Z_p is the charge number of the respective plasma species denoted by

p (= $e, i \cdots$), m_e the electron mass, m_t the test particle mass, Δt a time interval,

$$M_t = (m_t/m_e)^{3/2}\,(1+m_t/m_e)^{-1}\ ,\quad \chi_p = (m_p v^2/m_t v_\beta^2)T_p'^{-1},$$

$$\mu(\chi_p) = Erf(\sqrt{\chi_p}) - 2\sqrt{\chi_p/\pi}\ exp(-\chi_p)\ ,$$

$$v_\beta = \sqrt{2kT_{e0}/m_t}\ ,$$

and τ_s is the slowing-down time of test particles with mass number A_t and charge number Z_t at plasma center defined by

$$\tau_s = 0.125(A_t/Z_t^2)[T_{e0}(keV)^{3/2}/n_{e0}(10^{19}m^{-3})]\ . \qquad (3\text{-}12)$$

The summation $\sum$ in eqs. (3-8), (3-10) and (3-11) is taken for all the plasma species. The plasma parameters such as temperature T_p' and plasma density n_p' in the above expressions are normalized by the electron temperature T_{e0} and the electron density n_{e0} at the plasma center.

In the present Monte-Carlo simulation, Δv_l and Δv_t are computed by generating normal random numbers with the mean values and the mean square deviations given by eqs. (3-8) ~ (3-11) The Larmor phase Ω in eq. (3-6) is given by a uniform random number between zero and 2π.

(4) Simulation of charge exchange reactions

The charge-exchange process of fast ions is also simulated by a Monte-Carlo technique. The charge-exchange probability during a small time interval Δt is given by

$$P_{cx}(\Delta t) = 1 - exp(-n_0 <\sigma v>_{cx}\Delta t) \qquad (3\text{-}13)$$
$$\sim n_0 <\sigma v>_{cx}\Delta t$$

where n_0 is the neutral density, $<\sigma v>_{cx}$ the charge-exchange reaction rate of fast ions with back ground neutrals. To simulate the charge-exchange process, a simple hit-or-miss Monte-Carlo method is employed. The charge-exchange probability eq. (3-13) is calculated at every time step Δt for all the test particles, that is,

$$P_{cx}(\Delta t, i) \quad (i=1,2,\ldots\ldots,N_p) \ ,$$

where N_p is the total number of test particles. Simultaneously, N_p uniform random numbers

$$(\chi^{cx}_{random}(i), i=1,2,\ldots\ldots,N_p)$$

are also generated at every Δt. Comparing $P_{cx}(\Delta t, i)$ with $\chi^{cx}_{random}(i)$ for all the test particles, we switch on the calculation of charge-exchange process for only the particles whose $P_{cx}(\Delta t, i)$ is greater than $\chi^{cx}_{random}(i)$. Once a fast ion is charge-exchanged, it becomes a fast neutral and makes a straight flight in a plasma until it is reionized by the field particles or lost to the first wall. The reionization probability is described by

$$P_{ion}(s) = \int_0^s exp(-\lambda/\lambda_{ion})\, d\lambda/\lambda_{ion} \ , \qquad (3\text{-}14)$$

where λ is the flight length, λ_{ion} the ionization mean free path. The above integration is executed up to

$$\chi^{ri}_{random} = P_{ion}(s) \ ,$$

where χ^{ri}_{random} is another uniform random number between zero and unity. If a fast neutral hits the first wall without being reionized, it is labeled as a charge-exchange loss particle.

3.3 Calculation results

By using the above described Monte-Carlo code, one can obtain the following information;

1) loss fractions of NBI produced fast ions during slowing down due to charge exchange reactions, loss orbit and shine through,
2) fraction of total unthermalized beam power, and
3) profiles of NBI power deposited on plasma ions and electrons.

Calculations are made for plasma and NBI parameters appropriate to JT-60 which are summarized in Table 1 and 2, respectively. Figure 6 shows the

average density dependence of shine through, axi-symmetric orbit loss, charge exchange loss and unthermalized beam energy for JT-60. The total loss fraction of NBI power in JT-60 is about 10%. It must be noted that more than 10% of NBI power does not work to heat up the high temperature plasma. JT-60 employs an oblique injection. Therefore, the fraction of neutral beams ionized in the plasma central region reduces in proportion to the outward shift of the magnetic axis in a plasma with high β_p or in the divertor configuration of JT-60. Figure 7 shows the birth profiles of fast ions, (a) for the target plasma in limiter configuration with low β_p and (b) for the one in divertor configuration with high β_p, respectively. Because the magnetic axis is about 20 cm away from the beam axis in the divertor case (a), the deposition of fast ions in the central region becomes much smaller than that in the limiter case (b). The respective distributions of power deposition as a result of slowing down of fast ions are shown in Fig. 8-(a) and (b). The finite banana size of fast ions has an effect to level the uneven power deposition. For this reason, the deposition profiles are somewhat flat as compared with the birth profiles.

4. SCOOP : Time Slice Transport Analysis Code

There are frequently some differences between calculated results from an interpretation code and a prediction code. In those cases, we have had trouble with a problem whether two different kinds of codes have a common as a tokamak code. A code library system has been developed to organize and manage a large collection of computer codes used in the analysis of tokamak plasmas. This system provides us a great deal of benefit like that codes generated by the system have something in common among physical models and numerical calculation methods as tokamak codes. Therefore, when we come across a difference in results of the data analysis, we will easily find out the cause of it. The tokamak transport code library is referred to as 'LIBRARY'[15].

As one of interpretation codes produced from the LIBRARY, the SCOOP code performs the transport analysis of a tokamak plasma by solving the ion energy balance at a fixed time into a discharge. The schematic diagram of the code is shown in Fig.9. The input data to the SCOOP consist of profiles of electron density $n_e(r)$, electron temperature $T_e(r)$ and the radiated power $P_r(r)$, and the central ion temperature $T_i(0)$, together with the global parameters of plasma current I_p, surface voltage V_s and particle confinement time τ_p. The profiles of T_e, n_e, P_r and the beam power deposition are mapped to the magnetic surface by the LOOK/OFMC.

According to the input data, the magnetics field diffusion equation for the poloidal magnetic field is solved to evaluate the current density $J_z(r)$ and the effective charge number Z_{eff}. The particle flux is determined by the particle source of neutral beam in addition to the neutral density calculated on the basis of the particle confinement time.

In the steady transport analysis, the ion temperature profile is calculated by employing the neoclassical ion heat diffusivity proposed by Chang-Hinton[16] with a multiplication factor. The power transport between the electrons and the ions is calculated by the classical formula. The convective power loss is obtained from the inferred particle flux. As known the ion temperature diagnostic value, the multiplication factor could be adjusted to yield a central ion temperature in agreement with the measured one.

On the basis of above quantities, the electron heat diffusivity is estimated from the electron energy balance equation and the particle diffusion coefficient from the particle conservation equation.

4.1 Plasma resistivity

The resistive voltage, V_p, which is important to estimate the ohmic input power is defined by

$$V_s = V_p + \frac{1}{2} I_p \dot{L}_i \tag{4-1}$$

where L_i is the internal inductance. Although duration of JT-60 discharges is 10 sec, the effect of temporal evolution of L_i can not be neglected at a high plasma current(2 MA), leading to an uncertainty in the V_p of less than 20 %. From Shafranov $\Lambda(=\beta_p+l_i/2)$ evaluated by the equilibrium, the time derivative of L_i is expressed as

$$\dot{L}_i = \mu_0 R_p (\dot{\Lambda} - \dot{\beta}_p) \tag{4-2}$$

where μ_0 is the vacuum permeability and β_p the beta poloidal. As are assumed invariable profiles in time, the time evolution of β_p is approximated by

$$\dot{\beta}_p = \frac{1}{V}\int_0^a (\dot{p}_e(r) + \dot{p}_i(r))\mathrm{d}V/(B_p^2/2\mu_0) \tag{4-3}$$

$$\dot{p}_e(r) = \dot{n}_e(0) f_{ne}(r) T_e(r) + n_e(r)\dot{T}_e(0) f_{Te}(r),$$

$$\dot{p}_i(r) = \dot{n}_i(0) f_{ni}(r) T_i(r) + n_i(r)\dot{T}_i(0) f_{Ti}(r),$$

where $\dot{n}_e(0)$ and $\dot{T}_e(0)$ are measured by FIR and ECE diagnostics, respectively, and $f_n(r)$ and $f_T(r)$ are normalized profiles for the density and the temperature. The time derivative of ion pressure is approximated from the electrons, assuming $\dot{T}_i(0)=\dot{T}_e(0)$ and $\dot{n}_i(0)=\dot{n}_e(0)$.

The plasma resistivity $\eta_{\parallel}$ in the quasi-steady state is important in determining the electron energy balance of ohmically heated plasmas. As have been mentioned uncertainties in the plasma resistivity[17,18,19,20], two kinds of formula are used i.e. Spitzer resistivity and the neoclassical one with trapping correction[21]. In the calculation of the resistivity, the Z_{eff} is iteratively evaluated so that the resistive input power meets the input

power of I_pV_p, followed by

$$I_pV_p = \int_0^a \eta_{//}(Z_{eff},T_e(r))J_z(r)^2 dV. \tag{4-4}$$

In the following, we have used the two types of current density profiles. The first one is from the usual assumption of the constant electric field over the radius,

$$J_z(r) = \frac{E_z}{\eta_{//}(Z_{eff},T_e(r))}, \tag{4-5}$$

where $E_z=V_p/2\pi R_p$. Another model of $J_z(r)$ is represented by

$$J_z(r) = J_0(1-(\frac{r}{a})^2)^\alpha. \tag{4-6}$$

The central current density J_0 is given by assuming $q(0)\leqq 1$ and the value of α is adjusted to yield the Λ in agreement with the Λ_{FBI} from the FBI code. Both values of resistive Z_{eff} from two different J_z agree well in the case of small amount of scatter in measured $T_e(r)$. As is employed the eq.(4-5), the scatter of $T_e(r)$ leads to serious uncertainty in the resistive Z_{eff}. Therefore, the eq.(4-6) is preferred rather than the eq.(4-5).

We can now calculate the energy confinement time defined as

$$\tau_E = \frac{W_e+W_i}{V_pI_p+P_{NB}-(\dot{W}_e+\dot{W}_i)},$$

where W_e and W_i are, respectively, kinetic energies of the electron and the ion integrated over the plasma volume and P_{NB} is the absorbed power of the neutral beam.

4.2 Particle Balance

The particle balance equation is

$$\frac{\partial n_e}{\partial t} = -\frac{1}{r}\frac{\partial}{\partial r}(r\Gamma_e) + S_n + S_{NB} \tag{4-7}$$

where Γ_e is the particle flux, S_n the ion particle source and S_{NB} the neutral beam ionization source. The particle flux is determined by integrating eq. (4-7),

$$\Gamma_e(r) = \frac{1}{r}\int_0^r (S_n + S_{NB} - \frac{\partial n_e}{\partial t}) r dr. \tag{4-8}$$

The time derivative of density is determined from the experimental measurements as mentioned in section 4.1. The local particle sources, S_n and S_{NB} are calculated by a neutral penetration model code and the OFMC code. The normalized neutral density profile is obtained by the solution of Boltzmann equation[22] employing two models of neutral fluxes. The first is a cold neutral flux corresponding to puffing gas with the energy of 5 *eV*. The second is a warmer neutral flux corresponding to recycling particles the energy of which is taken as 5 *eV* for a divertor discharge and 50 *eV* for a limiter discharge[23]. The absolute magnitude of the neutral density is determined by the particle confinement time from $H\alpha$ measurements.

Ion density depletion is considered from the fast ion densities of neutral beam $n_f(r)$, and the Z_{eff} assuming a single species of impurity ion. The ion density profile is obtained from the condition of quasi-neutrality

$$n_e(r) = Z_i n_i(r) + n_f(r) + Z_k n_k(r), \tag{4-9}$$

in which Z_i is the ionic charge number and n_k the impurity ion density with the k-th charge number of Z_k. The impurity density is deduced by assumed an uniform profile of the Z_{eff}

$$n_k(r) = \frac{Z_{eff} - 1}{Z_k(Z_k - 1)} n_e(r). \tag{4-10}$$

The ion particle flux Γ_i is equated with the electron particle flux from the condition of ambipolar diffusion,

$$\Gamma_i(r) = \Gamma_e(r)/Z_i. \tag{4-11}$$

As is ignored the anomalous convective flow, the particle transport can be characterized by the anomalous diffusion coefficient,

$$D_A(r) = -\Gamma_e/\nabla n_e. \tag{4-12}$$

Figure 10-(a) shows profiles of the electron density(solid line), the ion density(dotted line) and the fast ion density (dashed line). The anomalous diffusion coefficient is shown in Fig.10-(b) for a neutral beam heated plasma, compared with the INTOR type scaling of $D_A(r)=1\times10^{19}/n_e(r)(m^2/s)$.

4.3 Ion Energy Balance

The steady state equation has been used in the transport analysis for the ion energy balance

$$-\frac{1}{r}\frac{\partial}{\partial r}(rq_i)+Q_{ei}+P_{NBi}-P_{CX}+P_n=0 \tag{4-13}$$

where q_i is the ion heat flux

$$q_i = -n_i\chi_i\frac{\partial T_i}{\partial r}+\frac{5}{2}T_i\Gamma_i \tag{4-14}$$

with the ion heat diffusivity,

$$\chi_i = C_\chi\chi_i^{CH}, \tag{4-15}$$

where χ_i^{CH} is the neoclassical ion heat diffusivity by Chang and Hinton multiplied by Z_{eff} and C_χ is an arbitrary multiplier varied so that the central ion temperature agrees with the experimental value. The Q_{ei} is given as the classical electron-ion energy equipartition term,

$$Q_{ei} = \frac{3}{2}n_e\frac{(T_e-T_i)}{\tau_{eq}} \tag{4-16}$$

where τ_{eq} is the electron-ion equipartition time including the effect of impurity collisions,

$$\tau_{eq} = \frac{3m_i(4\pi\varepsilon_0)^2 T_e^{3/2}}{8\sqrt{2\pi m_e}\, e^4 \sum_j (\frac{n_j}{n_e}\frac{Z_j^2}{A_j} \ln \Lambda_{ej})}, \tag{4-17}$$

in which the summation is taken over all ion species except fast ions and A_j is a mass ratio of j-specie ion. The neutral beam heating power absorbed into the ions, P_{NBi} is determined by the OFMC code. The charge-exchange loss term, P_{CX} due to thermalized ions, is defined as

$$P_{CX} = \frac{3}{2}(T_i - T_0) n_i n_0 <\sigma v>_{CX}. \tag{4-18}$$

The power gain and loss related with neutral particles by ionization and recombination is

$$P_n = \frac{3}{2} T_0 n_0 n_e <\sigma v>_{ioniz} - \frac{3}{2} T_i n_i n_e <\sigma v>_{recomb}. \tag{4-19}$$

With assumed ion heat diffusivity, the equation of (4-13) is solved to evaluate the ion temperature. Figure 11 shows integrated ion power flow profiles and both profiles of used ion heat diffusivity coefficient in a solid line and the one reversely deduced from the eq.(4-13) in a dotted line.

4.4 Electron Energy Balance

In the last stage of transport analysis procedure, the electron energy balance equation is solved to decide the electron heat diffusivity coefficient. The time-independent electron energy equation is

$$-\frac{1}{r}\frac{\partial}{\partial r}(rq_e) - Q_{ei} + P_J + P_{NBe} - P_R = 0 \tag{4-20}$$

where q_e is the electron heat flux

$$q_e = -n_e\chi_e\frac{\partial T_e}{\partial r}+\frac{5}{2}T_e\Gamma_e, \tag{4-21}$$

with the electron heat diffusivity coefficient χ_e. The P_J is the ohmic heating power density given by

$$P_J = \eta_{\parallel} j_z^2 \tag{4-22}$$

where $\eta_{\parallel}$ and j_z are obtained as described in the section 4.1. The P_{NBe} is the neutral beam heating power density absorbed into the electron calculated by the OFMC code. The P_R is decided by the sum of the ionization loss and the diagnostic radiative power loss P_r, from which the charge exchange loss should be subtracted,

$$P_R = P_r - P_{CX}+ \frac{3}{2}T_e n_e n_0 <\sigma v>_{ioniz}. \tag{4-23}$$

Integrating eq. (4-20), the electron heat diffusivity coefficient χ_e is determined consistently with the available data,

$$\chi_e(r) = \frac{\frac{3}{2}T_e\Gamma_e + \frac{1}{r}\int_0^r (Q_{ei}+P_R-P_J-P_{NBe})rdr}{n_e\frac{\partial T_e}{\partial r}}. \tag{4-24}$$

Figure 12 shows the profile of the electron heat diffusivity coefficient (solid line), comparing with the INTOR type scaling of $\chi_e=5\times10^{19}/n_e$ (dotted line) and integrated electron power flow profiles.

5. DARTS/RAC : Data bank/Regression Analysis Code

The transport analysis results are provided to a data bank of DARTS[24] that manages data of diagnosisses, operations and magnetic analysis results at a fixed time in a discharge. Since the DARTS includes a large amount of

where q_e is the electron heat flux

$$q_e = -n_e\chi_e\frac{\partial T_e}{\partial r}+\frac{5}{2}T_e\Gamma_e, \tag{4-21}$$

with the electron heat diffusivity coefficient χ_e. The P_J is the ohmic heating power density given by

$$P_J = \eta_{\parallel} j_z^2 \tag{4-22}$$

where $\eta_{\parallel}$ and j_z are obtained as described in the section 4.1. The P_{NBe} is the neutral beam heating power density absorbed into the electron calculated by the OFMC code. The P_R is decided by the sum of the ionization loss and the diagnostic radiative power loss P_r, from which the charge exchange loss should be subtracted,

$$P_R = P_r - P_{CX}+ \frac{3}{2}T_e n_e n_0 <\sigma v>_{ioniz}. \tag{4-23}$$

Integrating eq. (4-20), the electron heat diffusivity coefficient χ_e is determined consistently with the available data,

$$\chi_e(r) = \frac{\frac{3}{2}T_e\Gamma_e + \frac{1}{r}\int_0^r (Q_{ei}+P_R-P_J-P_{NBe})rdr}{n_e\frac{\partial T_e}{\partial r}}. \tag{4-24}$$

Figure 12 shows the profile of the electron heat diffusivity coefficient (solid line), comparing with the INTOR type scaling of $\chi_e=5\times10^{19}/n_e$ (dotted line) and integrated electron power flow profiles.

5. DARTS/RAC : Data bank/Regression Analysis Code

The transport analysis results are provided to a data bank of DARTS[24] that manages data of diagnosisses, operations and magnetic analysis results at a fixed time in a discharge. Since the DARTS includes a large amount of

data on JT-60 experiments up to now, we can easily produce any data base related to special plasma characteristics.

The data are investigated by using a code of RAC in order to find an over view of important consideration on the confinement. The RAC makes a non-linear regressive analysis between prominent data, in addition to the correlation among those. Figure 13[25] shows the regressive fitting on the plasma stored energy of JT-60 ohmic plasmas. The view of correlation between the plasma stored energy, the plasma current and the line averaged electron density is also presented. The details of the DARTS and the RAC will be described in elsewhere.

6. Concluding Remarks

The transport analysis code is very useful to infer an unknown quantity in a tokamak plasma, that is not yet determined by the diagnostic measurements, in addition to compare some theoretical works with the experimental transport coefficients, and to establish the confinement scaling for future tokamaks.

The tokamak experiment is now located at a new step that the break even condition would be attained by three large tokamaks of JT-60, TFTR and JET. In those large tokamaks, however, some experimental results which are different from ones found in medium or small tokamaks have been pointed out. This section will review such different points and the principle problems which remain to be solved.

The trapped electron plays an important role on the efficiency of the current drive through the plasma resistivity. Although the neoclassical resistivity with the trapped electron correction factor has been reported to explicate with experimental results of the current density profile, the safety factor and the surface voltage, the neoclassical resistive Z_{eff} in the JT-60[23] shows that the trapped electron correction factor should be reduced or suppressed, and the Z_{eff} value from the visible bremsstrahlung in the TFTR[26] lies between the neoclassical and Spitzer Z_{eff}'s. It is very important to directly measure the current profile, since the analysis results of the resistive Z_{eff} is very sensitive to the boundary electron temperature.

An anomalous inward flux of a form of $-2n_eD_Ar/a^2$ [27] is introduced so that the electron density profiles have a nearly parabolic or Gaussian shape

data on JT-60 experiments up to now, we can easily produce any data base related to special plasma characteristics.

The data are investigated by using a code of RAC in order to find an over view of important consideration on the confinement. The RAC makes a non-linear regressive analysis between prominent data, in addition to the correlation among those. Figure 13[25] shows the regressive fitting on the plasma stored energy of JT-60 ohmic plasmas. The view of correlation between the plasma stored energy, the plasma current and the line averaged electron density is also presented. The details of the DARTS and the RAC will be described in elsewhere.

6. Concluding Remarks

The transport analysis code is very useful to infer an unknown quantity in a tokamak plasma, that is not yet determined by the diagnostic measurements, in addition to compare some theoretical works with the experimental transport coefficients, and to establish the confinement scaling for future tokamaks.

The tokamak experiment is now located at a new step that the break even condition would be attained by three large tokamaks of JT-60, TFTR and JET. In those large tokamaks, however, some experimental results which are different from ones found in medium or small tokamaks have been pointed out. This section will review such different points and the principle problems which remain to be solved.

The trapped electron plays an important role on the efficiency of the current drive through the plasma resistivity. Although the neoclassical resistivity with the trapped electron correction factor has been reported to explicate with experimental results of the current density profile, the safety factor and the surface voltage, the neoclassical resistive Z_{eff} in the JT-60[23] shows that the trapped electron correction factor should be reduced or suppressed, and the Z_{eff} value from the visible bremsstrahlung in the TFTR[26] lies between the neoclassical and Spitzer Z_{eff}'s. It is very important to directly measure the current profile, since the analysis results of the resistive Z_{eff} is very sensitive to the boundary electron temperature.

An anomalous inward flux of a form of $-2n_eD_Ar/a^2$ [27] is introduced so that the electron density profiles have a nearly parabolic or Gaussian shape

in the inner region of the plasma column. In the JT-60, the flat density profiles with $n_e(0)/<n_e>=1.1\sim1.2$ are realized for middle- and high-density discharges, though peaked profiles like a parabolic shape are seen in limiter discharges at the low density. Without introducing the anomalous inward flux, the characteristics of the density profiles are satisfactory simulated by the difference in the neutral energy. Therefore, the anomalous inward flux is excluded from the particle transport analysis.

The particle confinement time is very important to estimate the particle flux and easily evaluated by the H_α measurements. However because of the large radial, poloidal and toroidal variations in the H_α intensities, the accurate estimation is very difficult. On the JT-60 divertor discharges, the particle confinement time has been well studied[28] due to the good homogeneity of the toroidal variations. The evaluated time is only 30ms for the NB heated plasmas, that causes a large amount of the charge exchange loss and makes it very difficult to clarify the insight of the energy balance on beam heated plasmas.

The ion temperature of the ohmically heated plasmas in the large tokamaks is very close to and strongly coupled with the electron temperature, because the energy confinement time is greater than the energy equipartition time between electrons and ions. Then, the energy equipartition is so strong that the usual procedure way to decide the enhancement factor to the neoclassical ion heat diffusivity coefficient is not appropriate to the plasmas with small differences in temperature between electrons and ions ; the required enhancement factor would be 50~100 to produce the ion temperature difference of 50eV in an ohmically heated, high density plasma. Even in beam heated plasmas, the terms of equipartition and convection are prominent in the ion energy balance. As evaluating the empirical ion heat diffusivity coefficient, we should pay close attention to the uncertainty in both the measurements and the numerical calculation, since the conduction term is only a small fraction of the ion energy balance.

Acknowledgements

The authors wish to thank Y. Shimomura, M. Azumi and T. Takizuka for their fruitful discussions through this work. The continuing support of S. Mori, K. Tomabechi, M. Yoshikawa and T. Iijima, is gratefully acknowledged.

in the inner region of the plasma column. In the JT-60, the flat density profiles with $n_e(0)/<n_e>=1.1\sim1.2$ are realized for middle- and high-density discharges, though peaked profiles like a parabolic shape are seen in limiter discharges at the low density. Without introducing the anomalous inward flux, the characteristics of the density profiles are satisfactory simulated by the difference in the neutral energy. Therefore, the anomalous inward flux is excluded from the particle transport analysis.

The particle confinement time is very important to estimate the particle flux and easily evaluated by the H_α measurements. However because of the large radial, poloidal and toroidal variations in the H_α intensities, the accurate estimation is very difficult. On the JT-60 divertor discharges, the particle confinement time has been well studied[28] due to the good homogeneity of the toroidal variations. The evaluated time is only 30*ms* for the NB heated plasmas, that causes a large amount of the charge exchange loss and makes it very difficult to clarify the insight of the energy balance on beam heated plasmas.

The ion temperature of the ohmically heated plasmas in the large tokamaks is very close to and strongly coupled with the electron temperature, because the energy confinement time is greater than the energy equipartition time between electrons and ions. Then, the energy equipartition is so strong that the usual procedure way to decide the enhancement factor to the neoclassical ion heat diffusivity coefficient is not appropriate to the plasmas with small differences in temperature between electrons and ions ; the required enhancement factor would be 50~100 to produce the ion temperature difference of 50*eV* in an ohmically heated, high density plasma. Even in beam heated plasmas, the terms of equipartition and convection are prominent in the ion energy balance. As evaluating the empirical ion heat diffusivity coefficient, we should pay close attention to the uncertainty in both the measurements and the numerical calculation, since the conduction term is only a small fraction of the ion energy balance.

Acknowledgements

The authors wish to thank Y. Shimomura, M. Azumi and T. Takizuka for their fruitful discussions through this work. The continuing support of S. Mori, K. Tomabechi, M. Yoshikawa and T. Iijima, is gratefully acknowledged.

References

1) Hawryluk, R.J. : *An Empirical Approach to Tokamak Transport*, Proc. of Physics of Plasmas close to Thermonuclear Conditions, EUR FU BRU/XII/476/80, (Brussels, 1979).
2) Wieland, R.M., Howe, H.C., Lazarus, E.A., Murakami, M., Thomas, C.E., ; Nucl. Fusion, 23 (1983) 447.
3) Azumi, M., Kurita, G. *et al.* : *A Fluid Model Numerical Code System for Tokamak Fusion Research*, Proc. of 4th Int. Symp. Computing Methods in Applied Sciences and Engineering, (Paris, 1979), 335.
4) Rome, J.A. *et al.* : Nucl. Fusion 14 (1974) 141.
5) Cordey, J.G. : Nucl. Fusion 16 (1976) 499.
6) Callen, J.D., Colchin, R.J., Fowler, R.H., McAlees, D.G., Rome, J.A. : Presented at 5th IAEA Conf. on Plasma Physics and Controlled Nuclear Fusion Research, Tokyo (1974), paper IAEA CN-33/A16-3.
7) Connor, J.W., Cordey, J.G. : Nucl. Fusion 14 (1974) 185.
8) Hively, L.M., Miley, G.H. : Nucl. Fusion 20 (1980) 969.
9) Ohtsuka, M., Tani, K., Kishimoto, H., Shimada, R., Yoshida, H., Hoshino, K., Tamura, S. : *Fast Ion Spatial Distribution in Neutral Beam Injection into a Tokamak*, JAERI-M 7551 (1978)
10) Olson, R.E., Salop, A. : *Stripped Ion Collision of Interest in MFE plasma Research, Stanford Research Institute Annual Report* (1977).
11) Nakai, Y. *et al.* : KAKUYUGO KENKYU, 39 (1978) 241.
12) Riviere, A.C. : Nucl. Fusion 11 (1971) 363.
13) Northrop, T.G. : *The Adiabatic Motion of Charged Particles* (Wiely, New York, 1963)
14) Turbnikov, B.A. : *Particle Interactions in a Fully Ionized Plasma*, Rev. Plasma Phys., Vol.1 (1965) 105.
15) Hirayama, T. : Presented at The Second US/Japan Work Shop on Transport Simulation in Large Tokamaks, (Princeton, 1985) ; T. Hirayama *et al.* : *Library System for a One Dimensional Tokamak Transport Code*, JAERI-M 82-204, (1982).
16) Chang, C.S., Hinton, F.L. : Phys. Fluids, 29 (1986) 3314.
17) BOL, K. *et al.* : in Plasma Physics and Controlled Nuclear Fusion Research (Proc. 7th Int. Conf. Insbruck, 1978), Vol.1, IAEA, Vienna (1979) 11.
18) Ejima, S., Petrie, T.W., Riviere, A.C. *et al.* : Nucl. Fusion, 22 (1982) 1627.

19) Meservey, E., Bitter, M., Daughney, C. : Nucl. Fusion, 24 (1984) 3.
20) Behringer, K.H., Abels-von Maanen, A., Bonnerus, J. *et al.* : in Plasma Physics and Controlled Nuclear Fusion Research (Proc. 10th Int. Conf. London, 1984), Vol.1, IAEA, Vienna (1985) 291.
21) Hirshman, S.P., Hawryluk, R.J., Birge, B. : Nucl. Fusion, 17 (1977) 611.
22) Tamor, S.J. : J. Comp. Phys. 40 (1980) 104.
23) Hirayama, T., Shimizu, K., Kikuchi, M., Shirai, H., JT-60 Team : *Transport Analysis of OH and NBI Heated Discharges in JT-60*, JAERI-M 87-029, (1987).
24) Aoyagi, T., ; private communication.
25) Kikuchi, M., Hirayama, T., Shimizu, K., Tani, K., *et al.* ; Nucl. Fusion 22 (1987) 1239.
26) Efthimon, P.C., Johnson, D.N., Bretz, N.L., Bitter, M., *et al.* : 14th European Conference on Controlled Fusion and Plasma Physics, (Proc. 14th Int. Conf. Madrid, 1987), Vol. 11D, EPS, Madrid (1987) 136.
27) Yamada, K., Tsuji, S., Shimizu, K., Nishitani, T., Nagashima, K., *et al.* : Nucl. Fusion 27 (1987) 1203.

Table 1 Plasma parameters

major radius	R_t = 3.04 m (limiter) 3.15 m (divertor)
minor radius	a = 0.93 m (limiter) 0.83 m (divertor)
toroidal field	B_t = 4.5 T at R = 3.04 m
plasma temperature	$T_e(\psi) = T_{e0}(1-(\psi_0-\psi)/\psi_0)$ ψ_0: ψ at plasma center
	$T_i(\psi) = T_e(\psi)$
	T_{e0} = 1.0 x 10^4 eV
plasma density	$n_e(\psi) = n_{e0}(1-((\psi_0-\psi)/\psi_0)^2)$
	n_{e0} = 0.1 to 1.1 x 10^{20} m^{-3}
safety factor	q_a = 2.5
plasma ion species	H^+
effective Z	Z_{eff} = 1.0 (uniform)

Table 2 Parameters of neutal beams in JT-60

beam energy	E = 75 keV
beam power	P = 20 MW
power ratio of neutral beam components	P_E : $P_{E/2}$: $P_{E/3}$ = 0.8 : 0.126 : 0.074
effective injection angle	θ_{inj} about +70 $deg.$ (co) +110 $deg.$ (counter)
injection scheme	P_{co} : $P_{counter}$ = 1 : 1
beam particle species	H^0

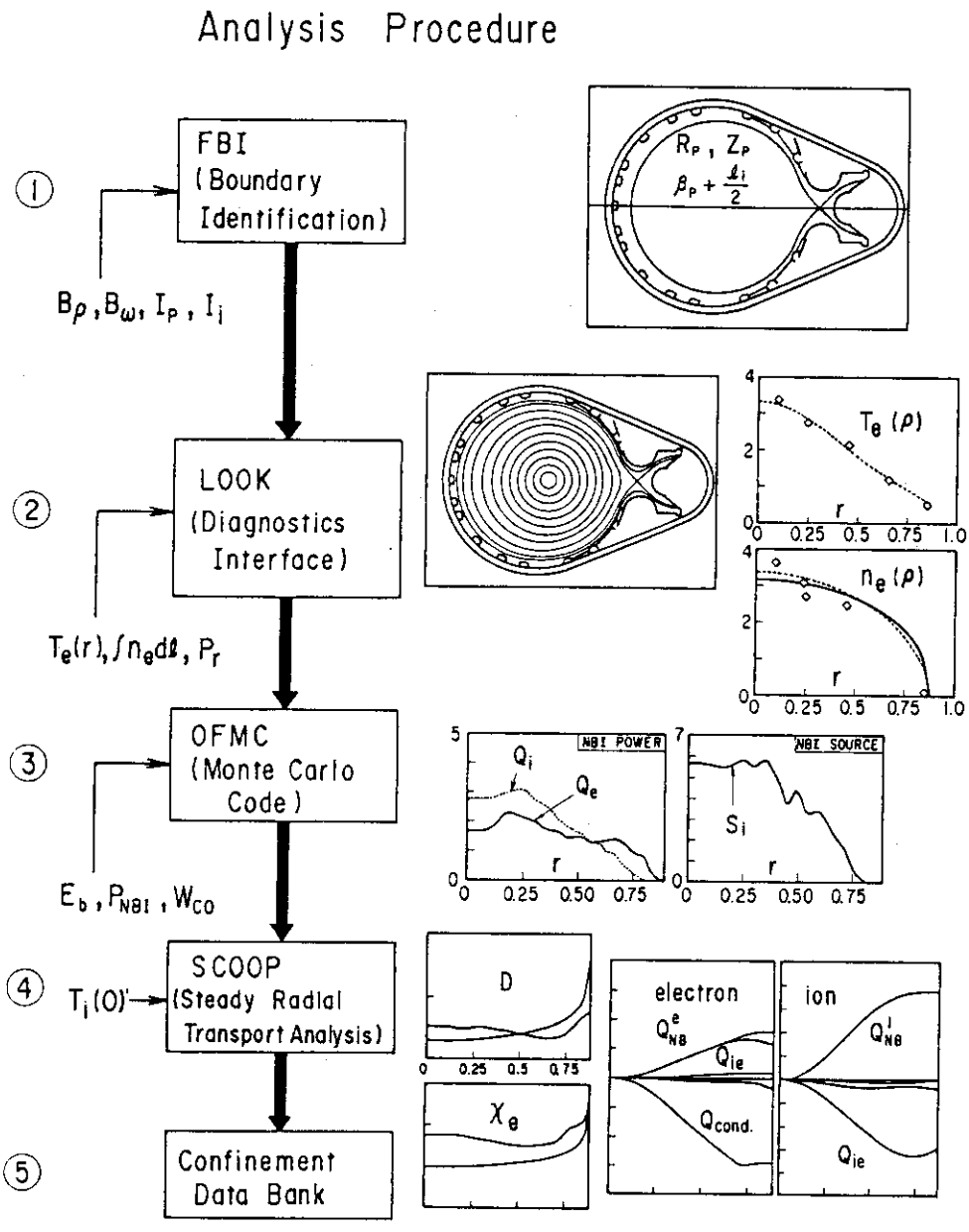

Fig.1 Rough sketch of the confinement analysis procedures. The plasma boundary is identified with FBI code. The internal flux surface is calculated with the numerical equilibrium code SELENE in which inner and outer plasma surfaces are matched to the FBI results. The radial profile of the diagnostics data such as T_e n_e and P_r are obtained by the least square fitting to the measurement as a function of the flux surface label. The particle and power deposition profiles of the injected neutral beam are calculated with the orbit following monte-carlo code. The transport coefficients such as χ_e, χ_i and D are obtained in 1-D radial transport analysis code SCOOP. Power balance of electron and ion, global parameters such as τ_E, W_s are also obtained in SCOOP. The analyzed data are stored in the confinement data bank.

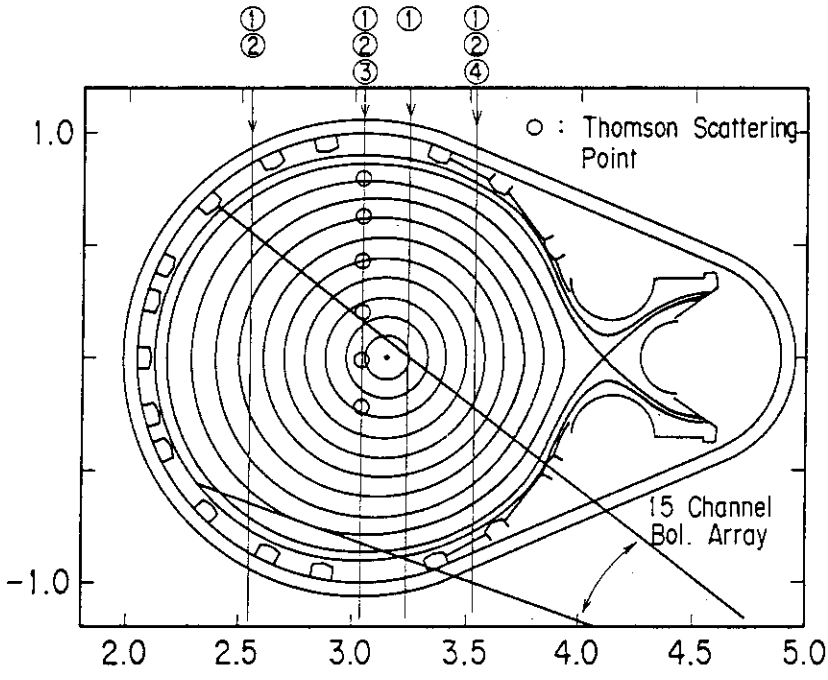

Fig.2 Typical equilibrium configuration and the diagnostics available for the confinement analysis in JT-60. Four channel interferometers are looking vertically (1) and 3 channel H_α detectors are used for τ_p measurement(2). The central ion temperature is measured by the crystal spectrometer, rutherford scattering of active He beam and charge exchange spectrum analyzer (3). Faraday rotation angle is also measured (4). A set of bolometer array is used for the radiation profile measurement.

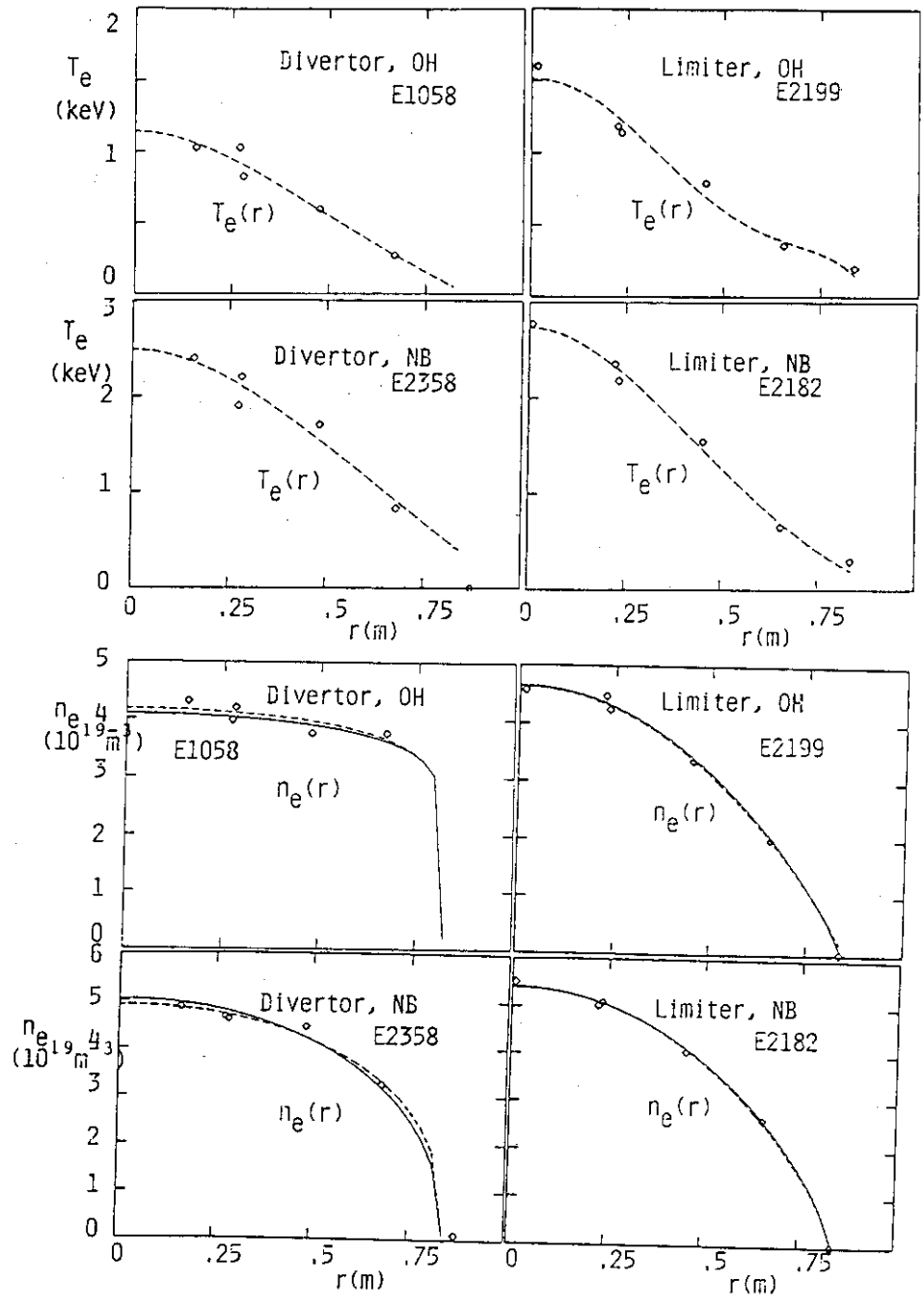

Fig.3 Typical temperature and density profiles during the ohmic and neutral beam heating. The broken lines are T_e and n_e profiles measured by the Thomson scattering. The solid lines are density profile obtained by the 4 channel interferometers.

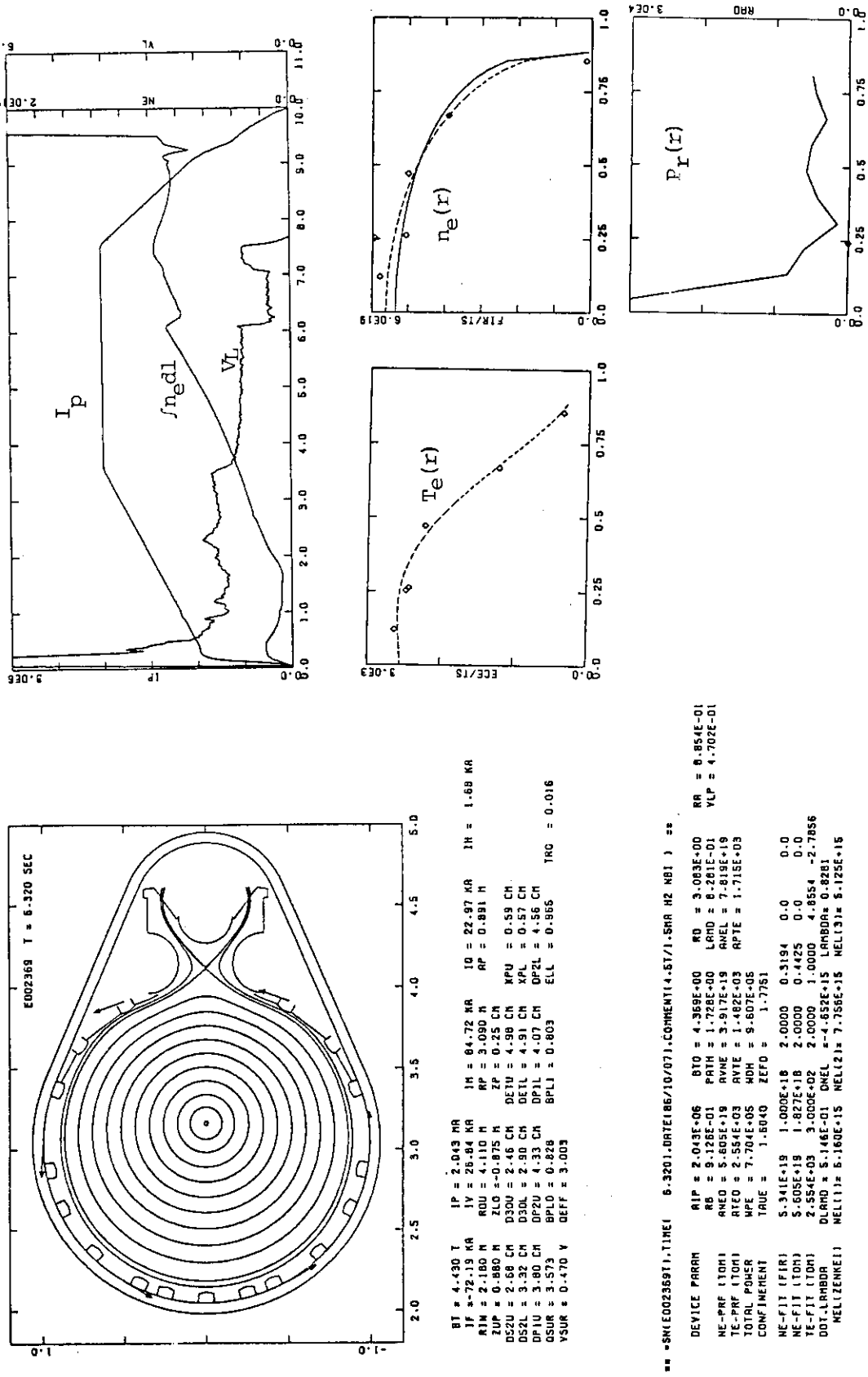

Fig.4 Typical output of LOOK code. Flux surface contour, magnetics parameters, profile parameters, discharge wave forms and T_e, n_e and P_r are given as an output.

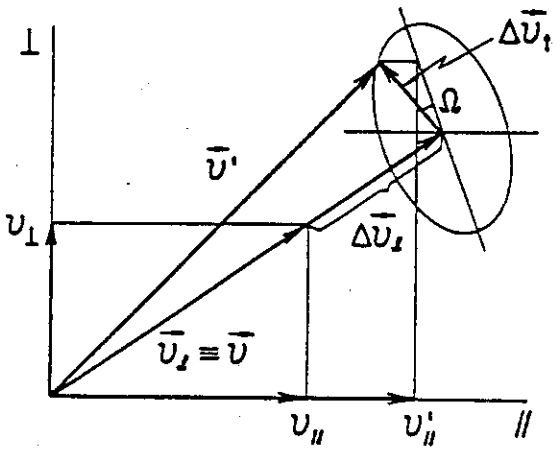

Fig.5 Schema for conversion of velocity change due to Coulomb collisions.

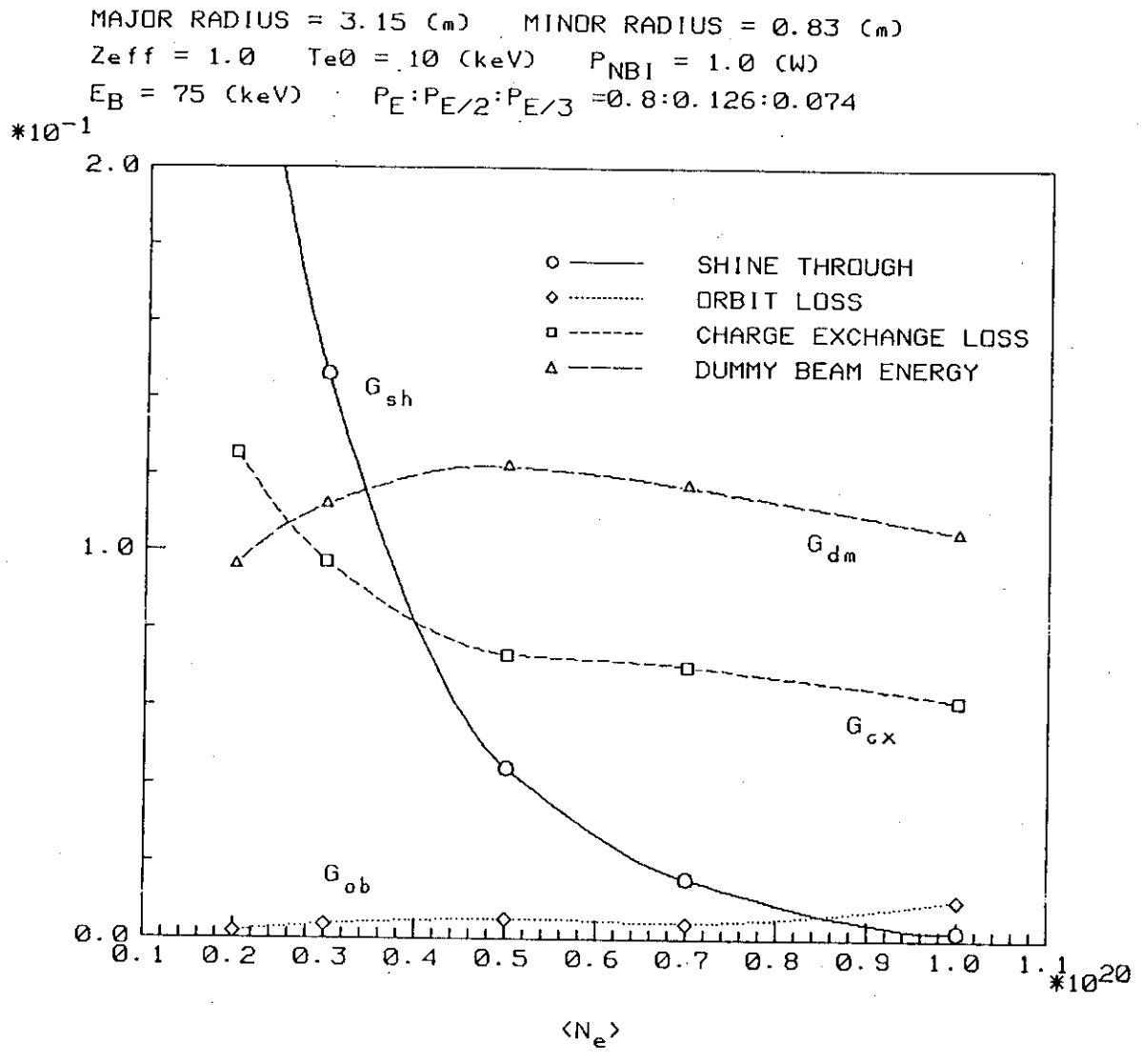

Fig.6 Average density dependence of shine through, axi-axi-symmetric orbit loss, charge exchange loss and dummy energy for JT-60.

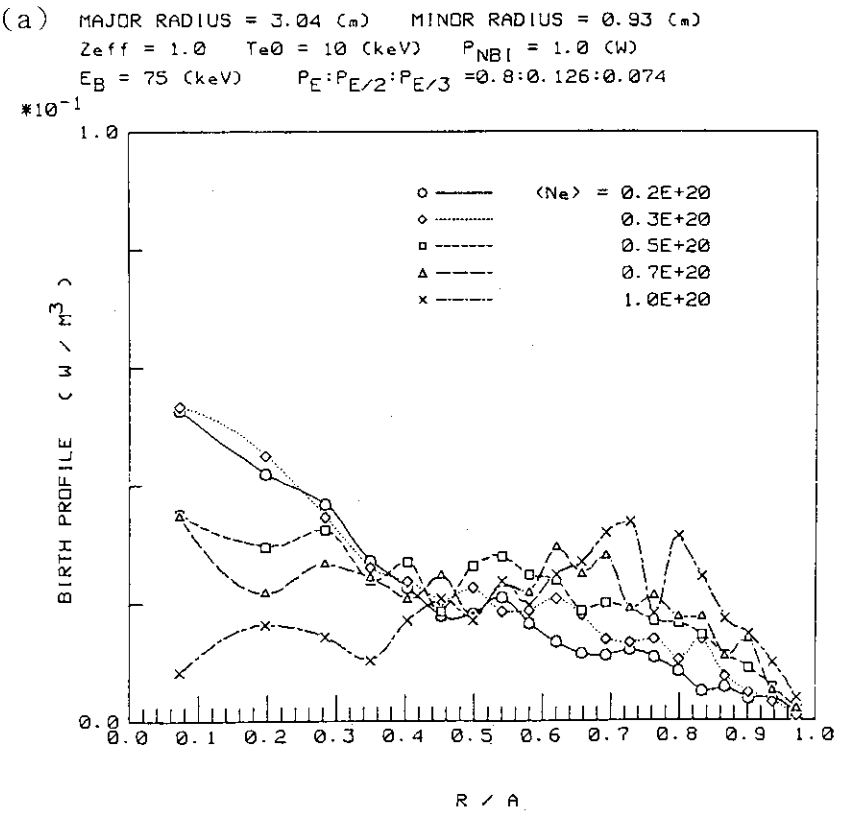

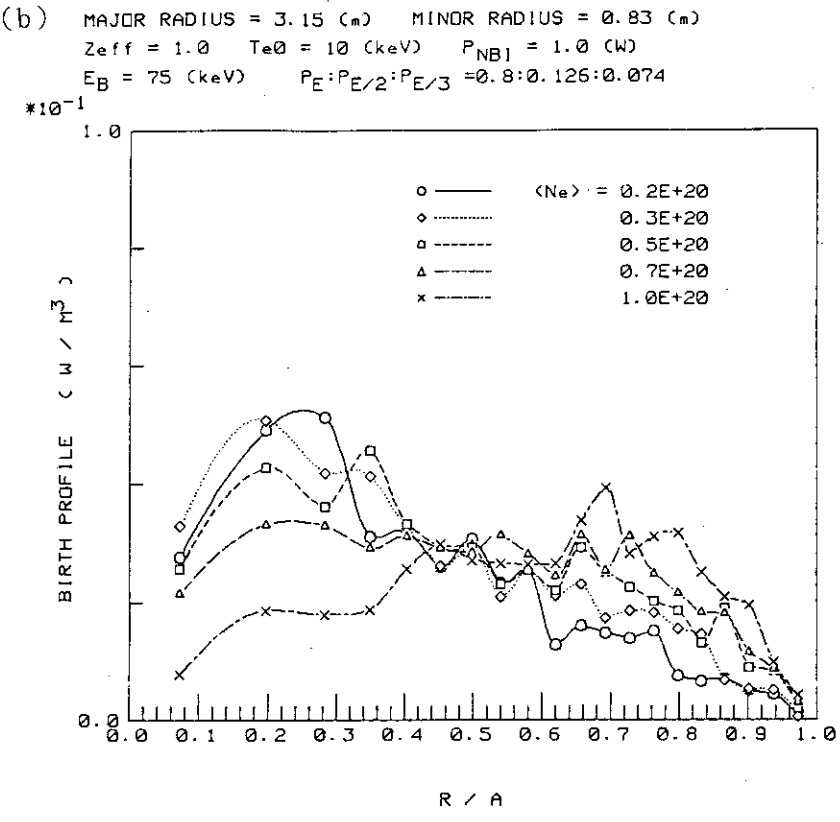

Fig.7 Birth profiles of fast ions, (a) for target plasma in limiter configuration with low β_p and (b) for the one in divertor configuration with high β_p.

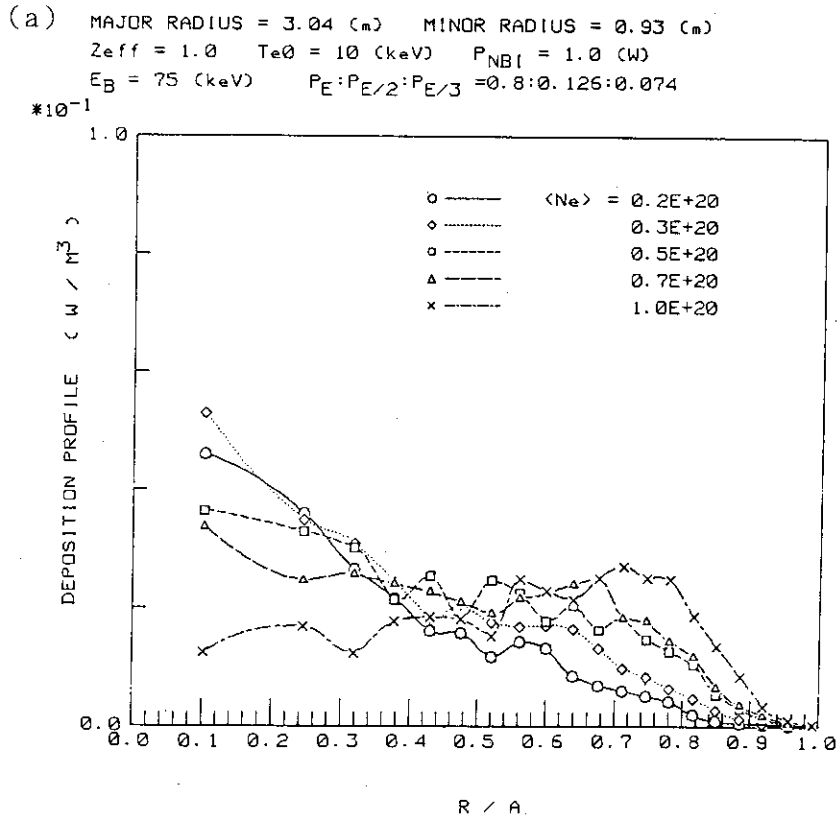

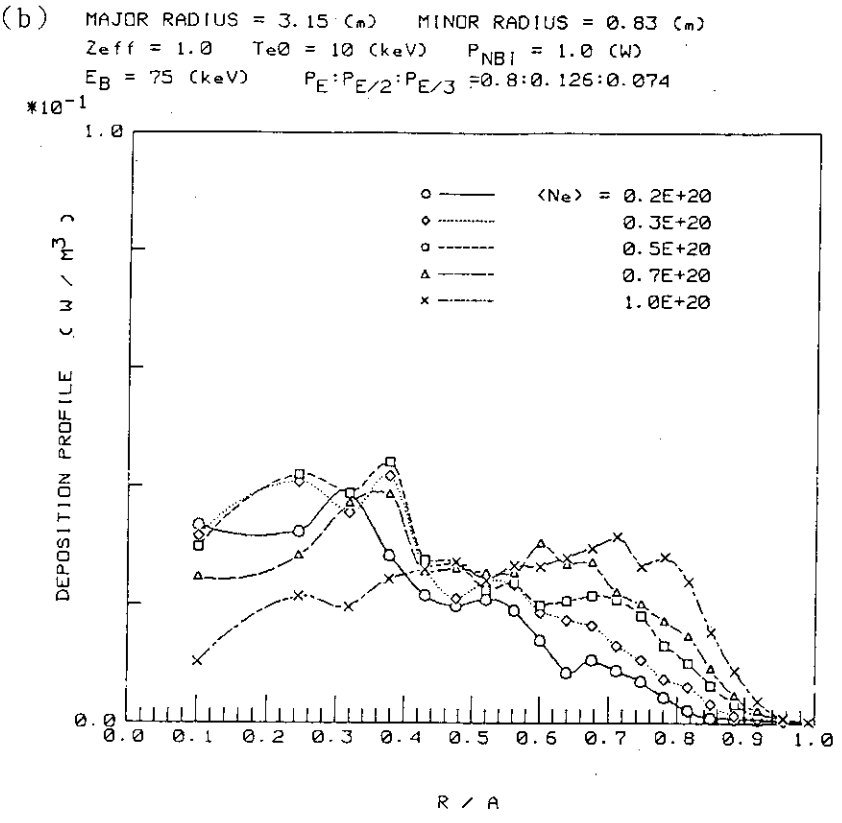

Fig.8 Distributions of power deposition of NBI, (a) for target plasma in limiter configuration with low β_p and (b) for the one in divertor configuration with high β_p.

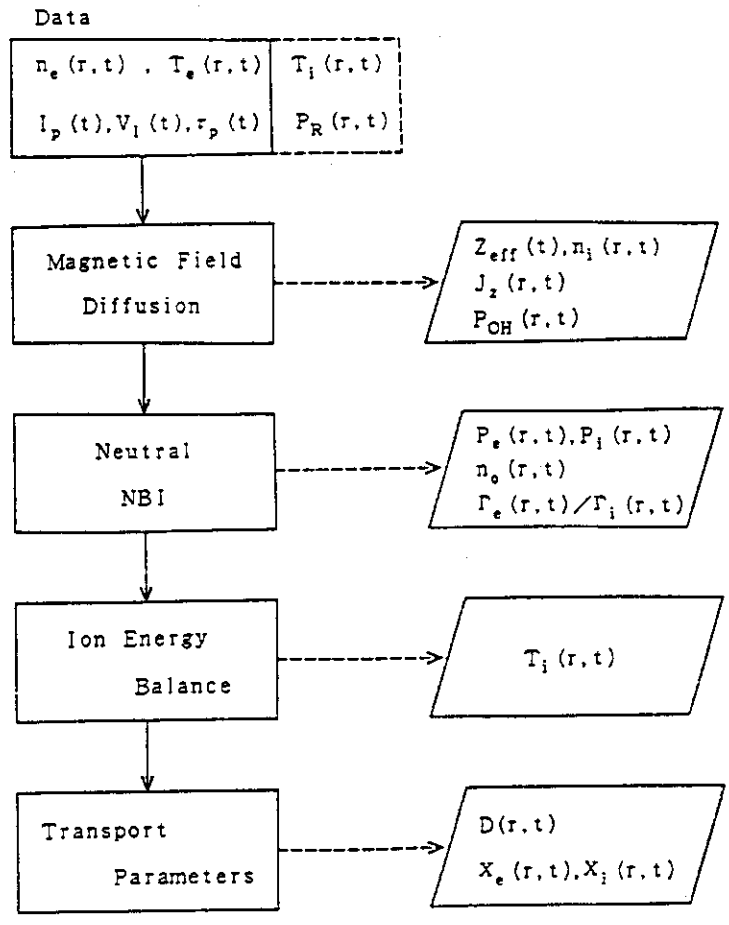

Fig.9 Structure of transport analysis code of SCOOP.

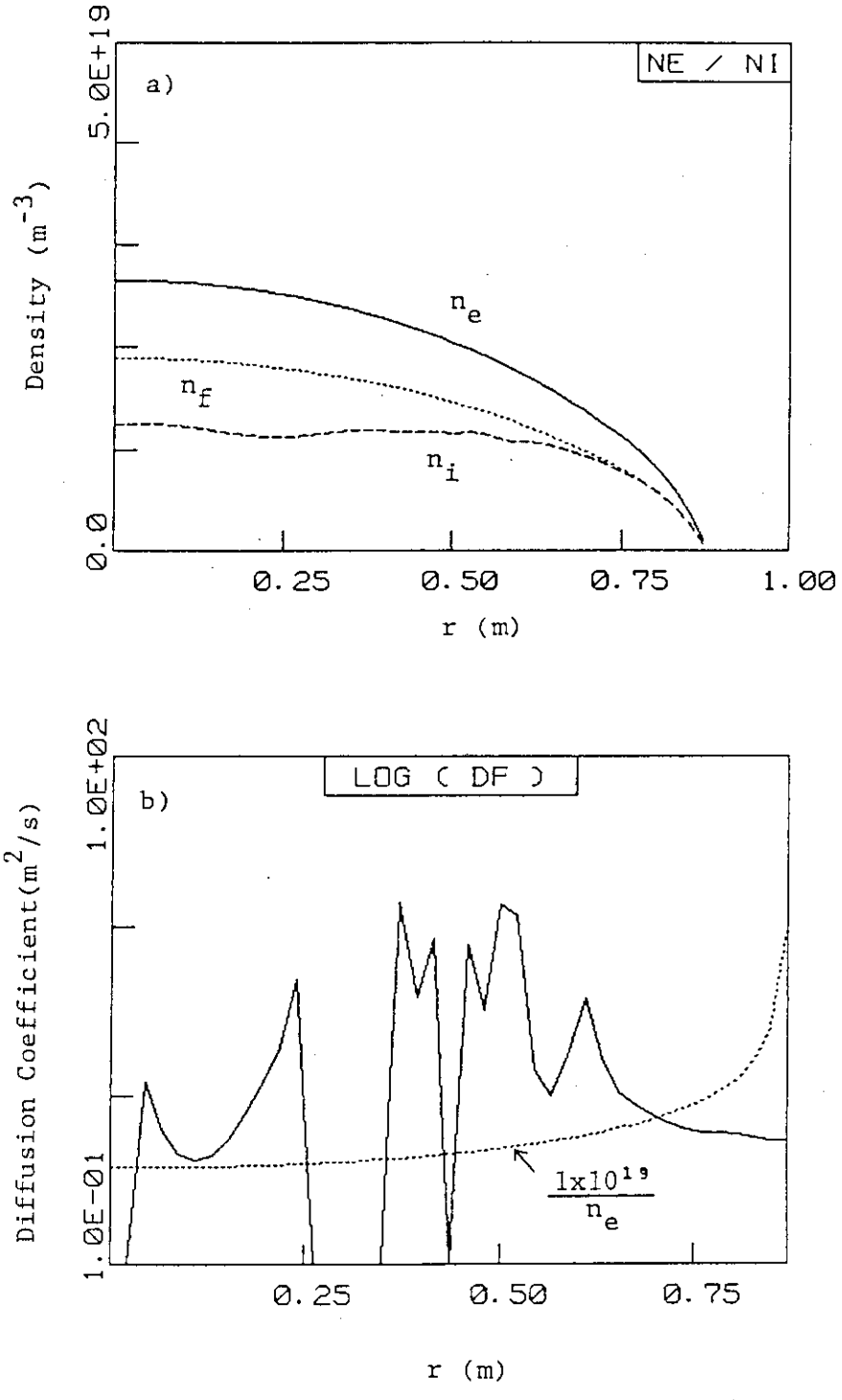

Fig.10 (a) Profiles of electron density (solid line), ion density (dotted line) and fast ion density (dashed line).
(b) The profile of anomalous diffusion coefficient deduced from diagnostic electron density profile, particle source of injected NB and background ion particle source. The solid line indicates the profile of anomalous diffusion coefficient, compared with the INTOR type scaling of $D_A=1\times10^{19}/n_e(r)$ shown in a dotted line.

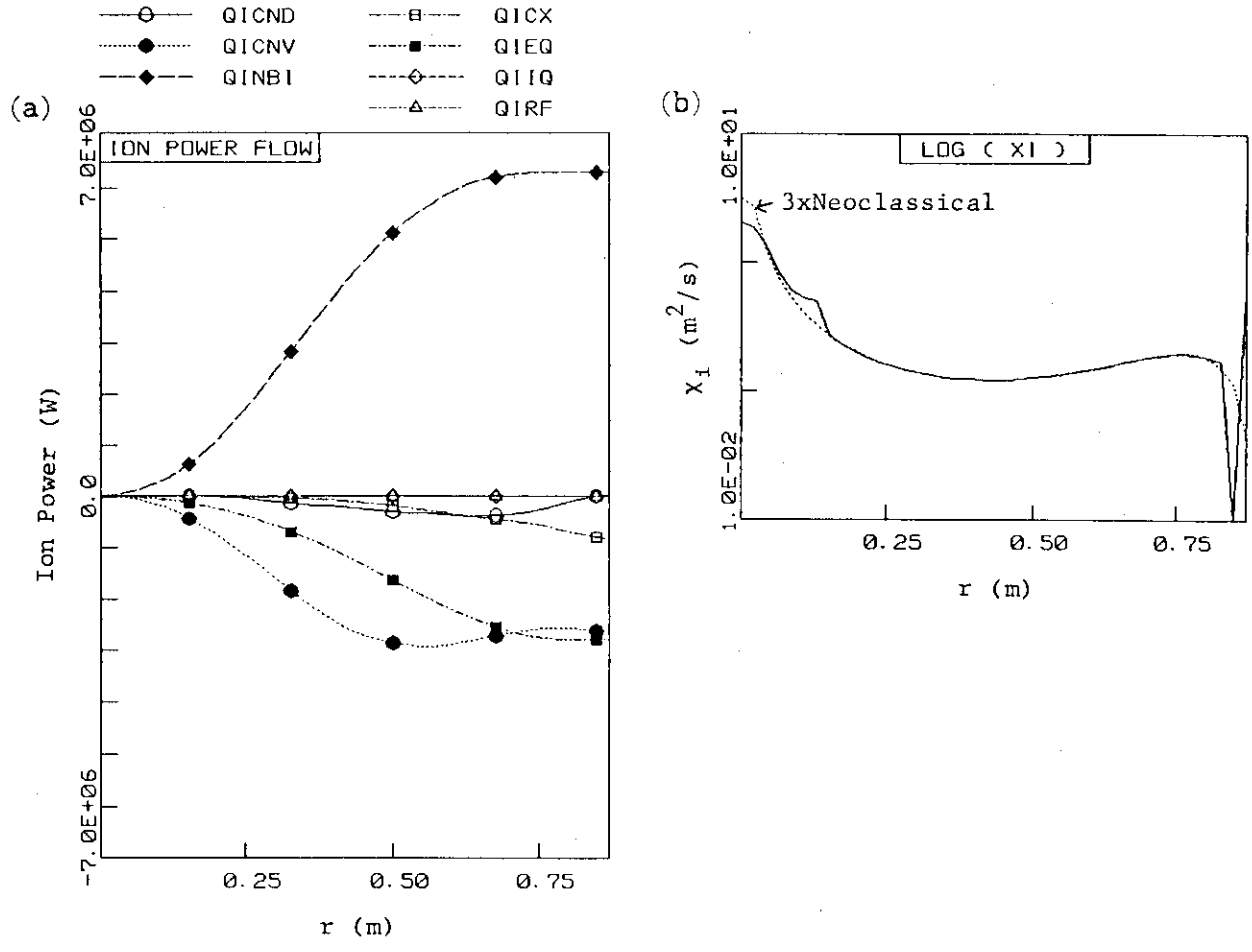

Fig.11 (a) The profile of volume integrated ion power flow versus a radius:
QICND ; ion conduction loss,
QICNV ; ion convection loss,
QINBI ; NB power deposited into ions,
QICX ; charge exchange loss,
QIEQ ; energy equipartition term between ions and electrons,
QIIQ ; energy equipartition term between ions and impurity ions,
QIRF ; RF power deposited into ions.
(b) Comparing between assumed ion heat diffusivity (solid line) and the one (dotted line) reversely deduced from the ion energy balance equation.

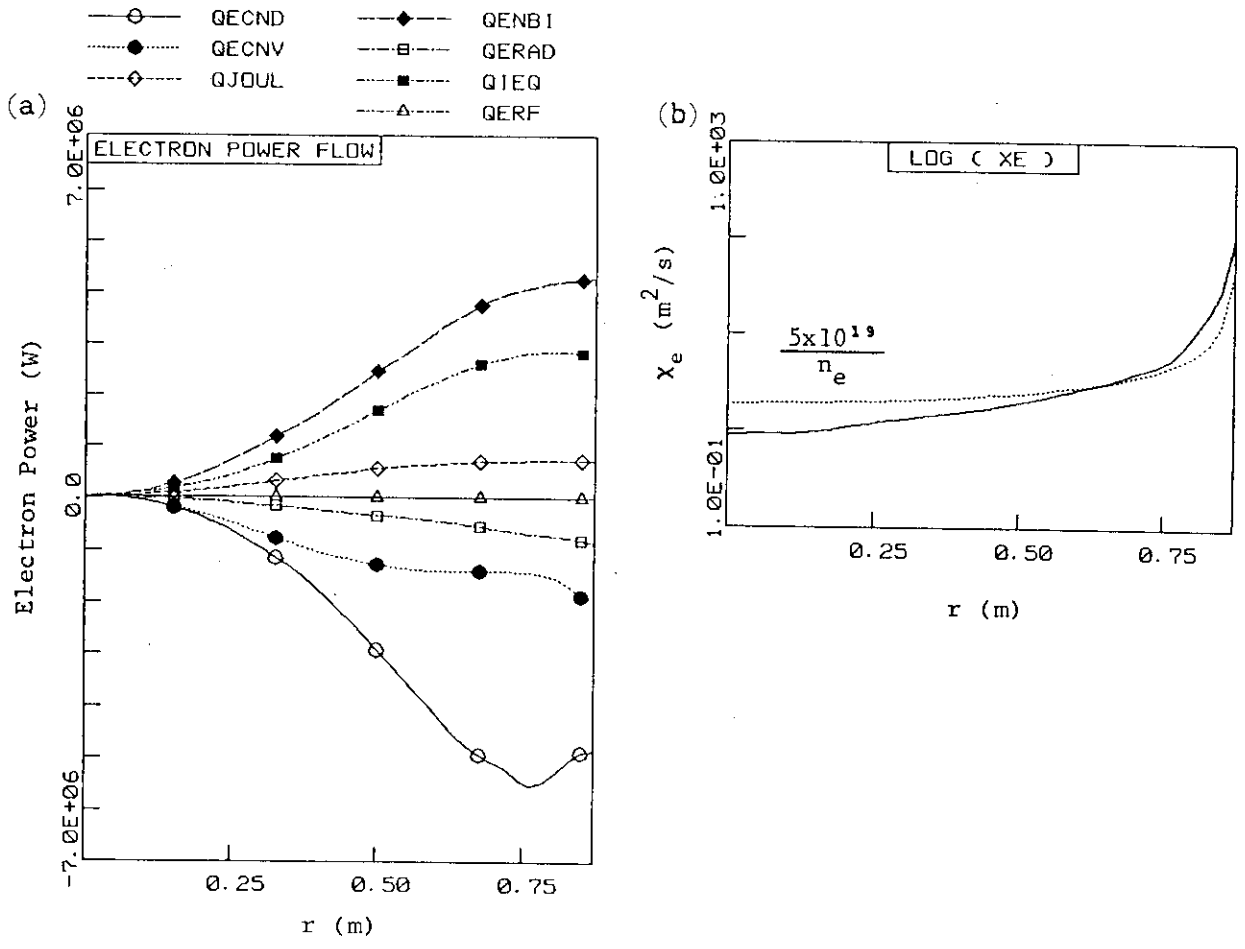

Fig.12 (a) The profile of volume integrated electron power flow versus a radius:

QECND ; electron conduction loss,
QECNV ; electron convection loss,
QJOUL ; Joule input power,
QENBI ; NB power deposited into electrons,
QERAD ; radiation loss,
QIEQ ; energy equipartition term between ions and electrons,
QERF ; RF power deposited into electrons.

(b) The profile of anomalous electron heat diffusivity (solid line) from deduced diagnostic profiles of electron temperature, density and radiation loss, and calculated results on power balance and NB heating. The INTOR type scaling of $\chi_i=5\times10^{19}/n_e$ is also presented in a dotted line.

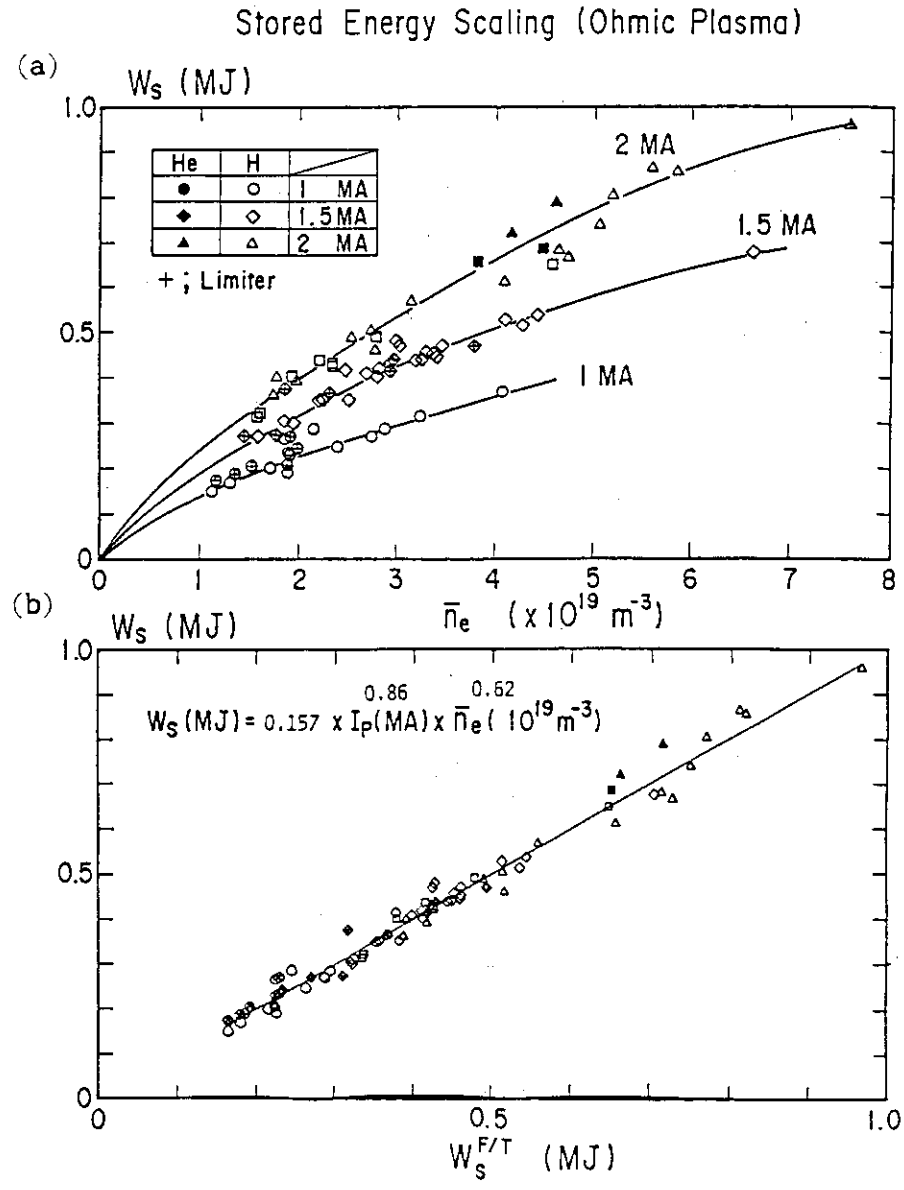

Fig.13 (a) Plasma stored energy during ohmic heating as a function of the electron density and the plasma current. (b) Regression fit of the stored energy W_s during ohmic heating as a function of the line averaged electron density $\bar{n}_e$ and the plasma current I_p. The experimental data are compared with the regression fit ($W_s^{scaling}$.)